*Water* **2014**, *6*, 1221-1245; doi:10.3390/w6051221

OPEN ACCESS

*water*

**ISSN 2073-4441**

www.mdpi.com/journal/water

*Article*

# Sensitivity of Distributed Hydrologic Simulations to Ground and Satellite Based Rainfall Products

**Singaiah Chintalapudi [1], Hatim O. Sharif [1,*] and Hongjie Xie [2]**

[1] Department of Civil and Environmental Engineering, University of Texas at San Antonio, One UTSA Circle, San Antonio, TX 78249, USA; E-Mail: chintalapudi4@gmail.com

[2] Department of Geological Sciences, University of Texas at San Antonio, One UTSA Circle, San Antonio, TX 78249, USA; E-Mail: hongjie.xie@utsa.edu

* Author to whom correspondence should be addressed; E-Mail: hatim.sharif@utsa.edu; Tel.: +210-458-6478; Fax: +210-458-6475.

*Received: 19 Ferauary 2014; in revised form: 13 April 2014 / Accepted: 25 April 2014 / Published: 7 May 2014*

**Abstract:** In this study, seven precipitation products (rain gauges, NEXRAD MPE, PERSIANN 0.25 degree, PERSIANN CCS-3hr, PERSIANN CCS-1hr, TRMM 3B42V7, and CMORPH) were used to force a physically-based distributed hydrologic model. The model was driven by these products to simulate the hydrologic response of a 1232 km$^2$ watershed in the Guadalupe River basin, Texas. Storm events in 2007 were used to analyze the precipitation products. Comparison with rain gauge observations reveals that there were significant biases in the satellite rainfall products and large variations in the estimated amounts. The radar basin average precipitation compared very well with the rain gauge product while the gauge-adjusted TRMM 3B42V7 precipitation compared best with observed rainfall among all satellite precipitation products. The NEXRAD MPE simulated streamflows matched the observed ones the best yielding the highest Nash-Sutcliffe Efficiency correlation coefficient values for both the July and August 2007 events. Simulations driven by TRMM 3B42V7 matched the observed streamflow better than other satellite products for both events. The PERSIANN coarse resolution product yielded better runoff results than the higher resolution product. The study reveals that satellite rainfall products are viable alternatives when rain gauge or ground radar observations are sparse or non-existent.

**Keywords:** satellite rainfall; NEXRAD; runoff; streamflow; GSSHA

## 1. Introduction

Accurate estimates of precipitation at different spatial and temporal scales are needed not only by weather forecasters and climate scientists, but also by hydrologists, agricultural engineers, and emergency personnel for a variety of application [1,2]. Rainfall is a key hydrologic variable for estimating the hydrologic response of a watershed as links the atmosphere with land surface processes. Consequently, accurate estimation of rainfall is necessary for hydrologic modeling as uncertainty in precipitation estimates greatly affects the model simulations and predictions. Furthermore, the representation of spatial and temporal variability of precipitation is crucial in hydrologic modeling. Rain gauges have problems in capturing the spatial variability of precipitation because they are point measurements. Tsintikidis [3] and Chintalapudi *et al.* [4] have shown that when rain gauges are sparsely distributed over the watershed, they will not be able to capture the spatial variability of rainfall needed for hydrologic modeling. In many practical applications rain gauges are unevenly distributed over the basin and interpolation is required to achieve reasonable spatial distribution of precipitation over the watershed [5,6]. The accuracy of precipitation values in between rain gauges solely depends on the interpolation technique.

Global satellite-based rainfall estimates are becoming increasingly available at higher spatiotemporal resolution (e.g., higher than 0.25 degree spatial resolution every 1 h or less) and temporal resolution of less than one hour. These products are suitable for fully distributed hydrologic models when rain gauges are nonexistent or sparse, especially in developing countries [2]. However, satellites have their own errors in estimating rainfall information, as many of these satellites have been in use since 1970. Researchers have developed different techniques to derive the precipitation data from the observations of satellites, which provide coverage for most of the globe [7–13]. Recent advances and development in technology has led to significant improvements of global and regional satellite-based precipitation products. As a result, the applicability of these products into large-scale distributed hydrologic models has been increasing in recent years. The accuracy of satellite-based rainfall estimates have been increasing over the years due to the new techniques that merge different satellite, radar, and rain gauge products to produce better rainfall estimates [14].

The National Weather Service (NWS) River Forecast Center (RFC) has developed a product, called MPE (Multi-sensor Precipitation Estimator) that combines NEXRAD raw data with rain gauge and satellite data. Numerous studies have conducted inter-comparisons between MPE precipitation estimates and rain gauge observations (e.g., [4,15–21]). These studies showed that the calibrated radar products such as NEXRAD Stage III and MPE yielded more accurate streamflows than the rain gauge network alone. However, Smith *et al.* [22] found that Weather Surveillance Radar (WSR-88D) rainfall significantly underestimated the rainfall when compared to rain gauge rainfall. Smith *et al.* [22] also concluded that the accuracy of rainfall products degraded at far ranges (150 km in spring-summer and 100 km in winter-fall). Young *et al.* [23] found that beam blockage is a serious problem that is not corrected by existing NEXRAD algorithms in mountain areas.

Numerous researches have used different rain gauge and remote sensing precipitation datasets in hydrologic modeling, such as NEXRAD Stage III, Multi Sensor Precipitation Estimator (MPE), Tropical Measuring Mission (TRMM), Precipitation Estimation from Remotely Sensed Information (PERSIANN), and CPC MORPHing Technique (CMORPH), in various regions of the world

(e.g., [1,2,4,6,7,24–32]). However, these studies do not agree on what the best precipitation data set is for hydrologic modeling. For example, Chintalapudi *et al.* [4] found that a dense rain gauge network (one rain gauge for every 97 $km^2$ of basin area) significantly underestimated the streamflows for the June 2002 storm event over the Upper Guadalupe River Basin. Tsintikidis *et al.* [3] also concluded that rain gauge precipitation underestimated the streamflows in Folsom Lake Watershed. However, other studies concluded that dense rain gauge networks provided superior model performance (e.g., [33]).

Collischonn *et al.* [34] concluded that TRMM rainfall product was the best rainfall data set to model streamflows in the Amazon catchment, whereas Nesbitt *et al.* [35] showed that CMORPH and PERSIANN estimated higher rainfall rates than TRMM rainfall product in the Sierra Madre Occidental. Dinku *et al.* [27] found that CMORPH and TRMM rainfall products performed relatively better over Ethiopia and Zimbabwe. In South America, de Goncalves *et al.* [36] demonstrated that PERSIANN performed better than TRMM rainfall product. Gourley *et al.* [30] analyzed unadjusted NEXRAD, NEXRAD Stage IV, PERSIANN Cloud Classification System (CCS), rain gauge, and TRMM Multisatellite Precipitation Analysis (TMPA) products over the Ft. Cobb basin in Oklahoma, which has a high density rain gauge network. Gourley *et al.* [37] concluded that unadjusted NEXRAD rainfall is the worst product while NEXRAD Stage IV has the best hydrologic skill in estimating streamflows, and the simulations driven by the TRMM product were better than those provided by the PERSIANN CCS product. Jiang *et al.* [38] showed that CMORPH simulations were much better than TRMM 3B42V6 simulations over the Laohahe Basin in Northern China.

In this study, satellite-derived precipitation datasets including NEXRAD MPE, TRMM 3B42V7, CMORPH, PERSIANN CCS 1-h, PERSIANN CCS 3-h, PERSIANN 0.25 degree, and rain gauge products were used as input to a physically-based fully distributed hydrologic model. The main objective of this study was to assess the hydrologic skill of each precipitation dataset in simulating the watershed response in a sub-basin of the Guadalupe River watershed. This study also analyzed the spatial variability of infiltration and runoff characteristics over the basin.

## 2. Study Area

The watershed selected for this study is the Guadalupe River watershed above Canyon Lake and below Comfort, Texas. The watershed has an area of 1232 $km^2$. The USGS 08167500 stream gauge located near Spring Branch, Texas was selected as an outlet for this watershed (Figure 1). The mean elevation of the basin is about 442.3 m above mean sea level, the slope of the basin is 0.05, the watershed length is 58.2 km, and the maximum flow distance to the outlet is about 102 km. The watershed passes through Kerr, Comal, Kendall, and Blanco counties, but the most of the watershed is located in Kendall County. The average annual rainfall in the study area is approximately 813 mm. The annual average minimum and maximum temperatures are about 5 and 35 °C, respectively. Urban area, cattle, goat, and sheep production, as well as light and heavy industry are the major land uses in the study area [39]. The outflow from this basin goes directly into Canyon Lake.

**Figure 1.** Location of the study area in Texas.

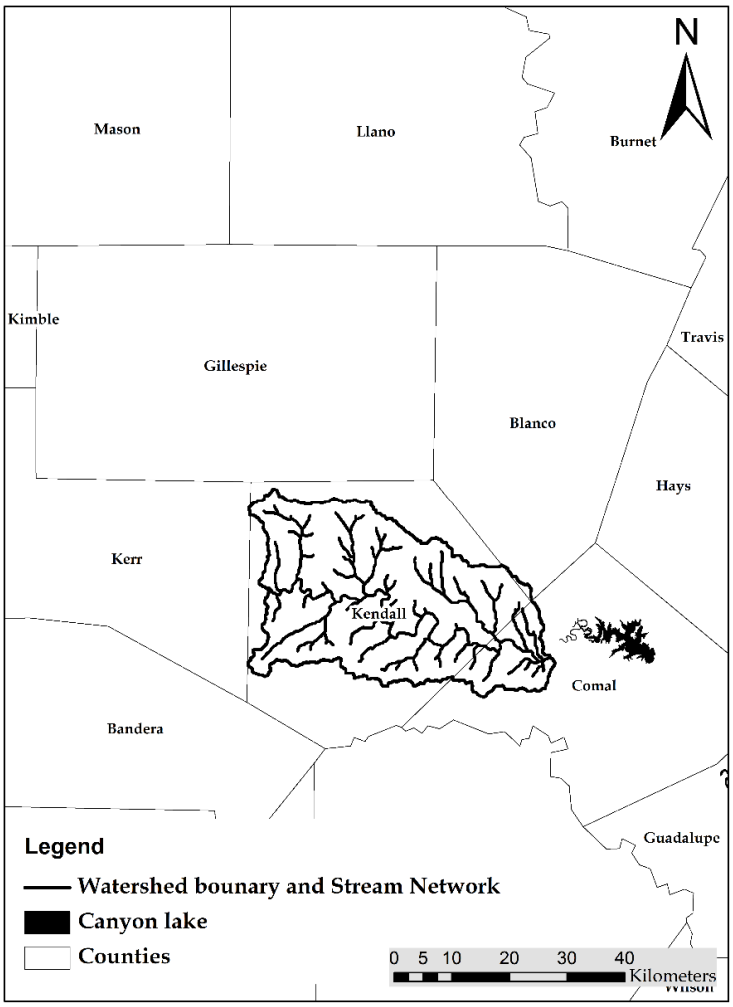


## 3. Hydrologic Model

The physically-based distributed hydrologic model Gridded Surface Subsurface Hydrologic Analysis (GSSHA) was selected to perform this study [40]. GSSHA model has been used to study different flooding events, including the 2002, 2004, and 2007 storm events in San Antonio, Texas [23,41], the June 2002 storm event in the upper Guadalupe River watershed [4], and the November 2004 flooding event in the middle Guadalupe River watershed and Bull Creek watershed, Austin, Texas [18,19].

GSSHA is a fully distributed hydrologic model based on equally sized square grid cells. The hydrologic parameters that influence the watershed response are specified for each grid cell, resulting in a fully distributed-parameter hydrologic model. No calibration was made as GSSHA uses physics-based partial diffusive wave equations which describe the runoff processes from each grid cell and channel reach in order to model the watershed response under given conditions. In this study, the Alternative Direction Explicit (ADE) method was used to calculate the 2D overland flow, the Green and Ampt with Redistribution (GAR) method was used to calculate infiltration into the soil, and diffusive wave equations was used to calculate 1D channel flow from each grid cell. A time step of 20 s was adopted in this study. GSSHA model grids are built on a Digital Elevation Model (DEM) of

the watershed with a cell size that can typically vary from 10 to 1000 m. The model was developed using the Watershed Modeling System (WMS) interface [42]. The input files for the GSSHA model are a series of text files in the form of a gridded GRASS ASCII format. The project file specifies the basin operational model settings which are overland flow routing, channel routing, and infiltration methods, and stores the pathways of input text files such as land cover, soils, and precipitation.

## 4. Storm Events

The July 2007 and the August 2007 storm events were used to evaluate the different precipitation products and use these products to force the GSSHA model simulations over the basin. In 2007, Texas had its wettest summer on record and Oklahoma its fourth wettest [43]. The summer 2007 rainfall in south central Texas, especially in the Hill Country region, resulted in Major River flooding. July 2007 received a significant amount of rainfall that led authorities to issue hundreds of flash flood warnings. By the end of July 2007, most river locations had exceeded their flood levels at least once [44]. Figure 2 shows the spatial distribution of July 2007 monthly observed precipitation. The southeastern portion of Texas received higher amounts of rainfall. The July 2007 rainfall in the study area (watershed boundary shown) varied from 127 to 381 mm (Figure 2). The upstream portion of the watershed received approximately 127 mm of rainfall while the downstream portion of the basin received about 381 mm of rainfall.

**Figure 2.** July 2007 observed precipitation [44].

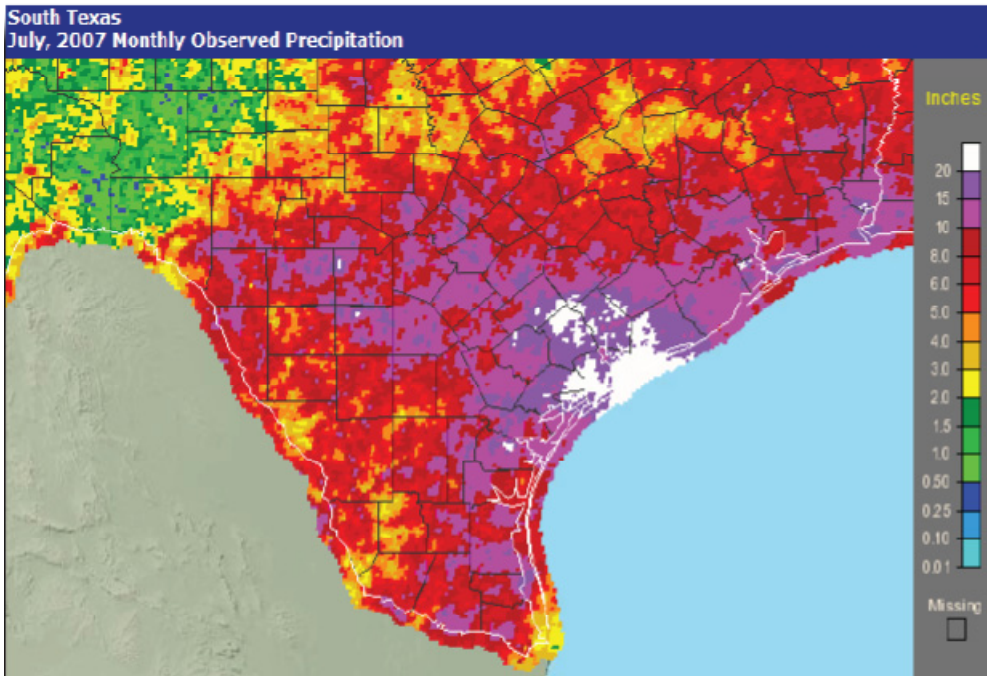


Tropical Storm Erin made landfall on the Texas coast in the Port Arkansas area bringing large amounts of rain to the western portions of Texas on 17–18 August 2007. Although it was not a big storm, Storm Erin unleashed torrential rains over the southern plains as it moved inland on 16–19 August 2007. Heavy rainfall totals of about 100 to 200 mm were recorded in the landfall area, as well as in central Oklahoma where Erin persisted as a prolonged tropical depression that caused 200

to 250 mm of rainfall. The upstream portion of the basin received rainfall ranging from 50 to 100 mm while the downstream portion received 25 to 50 mm of rainfall during Tropical Storm Erin (Figure 3).

**Figure 3.** 10–20 August 2007, rainfall totals recorded by the TRMM satellite [45].

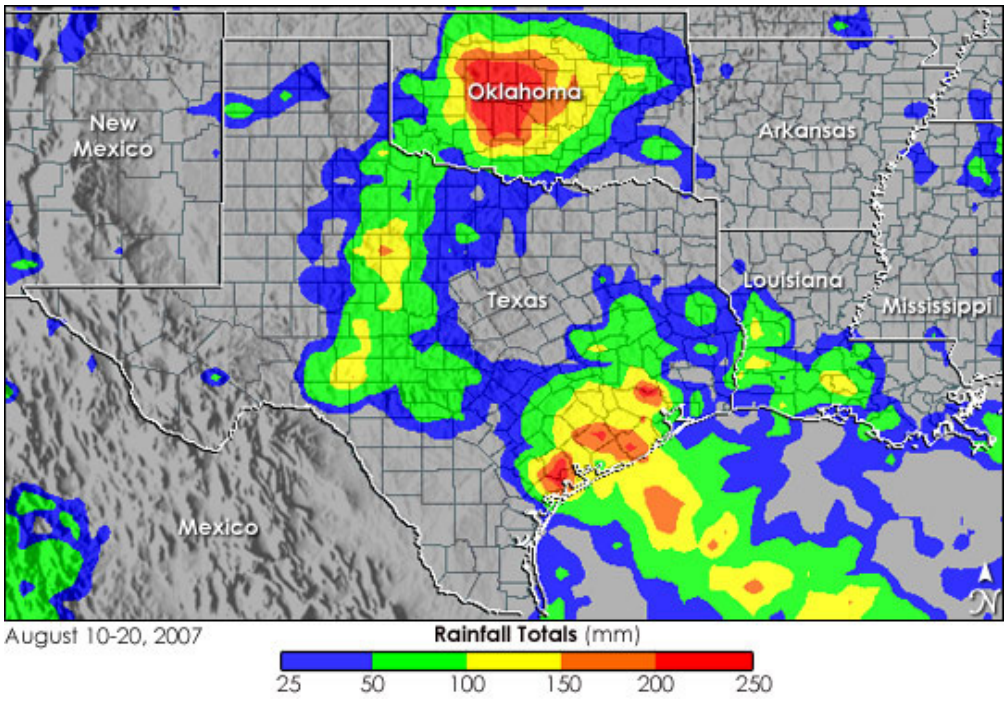


## 5. Watershed Data

The US Geological Survey (USGS) 30-m Digital Elevation Models (DEMs) were downloaded from the USGS National Map Viewer website. The initial processing, such as defining the projection, resampling 30 m DEM to 150 m DEM (GSSHA model grid cell size), and clipping to the study area were performed using ArcGIS 10.0 software. Later, WMS (Watershed Modeling System) software was used for delineation of the stream network and watershed using the 150 m DEM. Smoothing and filling processes were performed on the 150 m DEM in WMS to avoid errors. The TOPAZ tool in WMS was used to delineate the stream network, which was then compared to the USGS National Hydrography Dataset (NHD) to check the accuracy and to adjust the minor errors caused by the delineation process. The USGS 08167500 stream gauge located near Spring Branch, Texas was selected as the outlet when delineating the basin. This process resulted in a drainage basin area of 1232 $km^2$ (Figure 1). The WMS includes the Cleandam tool to fill pits, depressions, and remove digital dams in the original DEM.

### *5.1. Land Cover and Soils*

The land use/cover and soil type maps and metadata were downloaded from USGS and US Department of Agriculture (USDA) websites. These datasets were processed in ArcGIS to create GSSHA input files which represent the physical characteristics of the watershed. The state soil geographic database (STATSGO) was used to derive the soil types. The Soil Data Viewer (SDV) software, available at the USDA website, was used to derive the soil types. Shrub land is the dominant land cover in the watershed (44.79%). Shrub lands are distributed throughout the watershed, but the

intensity is higher in the upstream portion. Forest is the second largest land cover (36.62%), followed by grasslands (15%), developed areas (2.44%), cultivated crops (0.55%), pasture (0.45%), open water bodies (0.08%), woody wetlands (0.05%), and barren land (0.01%), (Table 1, Figure 4). The forest land cover intensity is high near the outlet and distributed throughout the watershed. The cultivated crop land cover areas are along the main stream channel in the upstream portion of the watershed. Clay loam is the dominant soil (45.93%) followed by clay (25.54%), very cobbly clay (18.89%), and silty clay (9.64%), (Table 2, Figure 5). Clay soil is deposited near the outlet, very cobbly clay is located in the upstream portion of the basin, silty clay is found along the stream channels of the watershed, and clay loam is deposited throughout the watershed (Figure 5).

**Table 1.** Different land cover types and their percentages in the watershed.

| Land use | % Land use in the watershed |
|---|---|
| Open water | 0.08 |
| Developed areas | 2.44 |
| Barren land (rock/sand/clay) | 0.01 |
| Forest | 36.62 |
| Shrub/scrub | 44.79 |
| Grassland/herbaceous | 14.99 |
| Pasture/hay | 0.46 |
| Cultivated crops | 0.55 |
| Woody wetlands | 0.05 |

**Figure 4.** Different land covers in the study area.

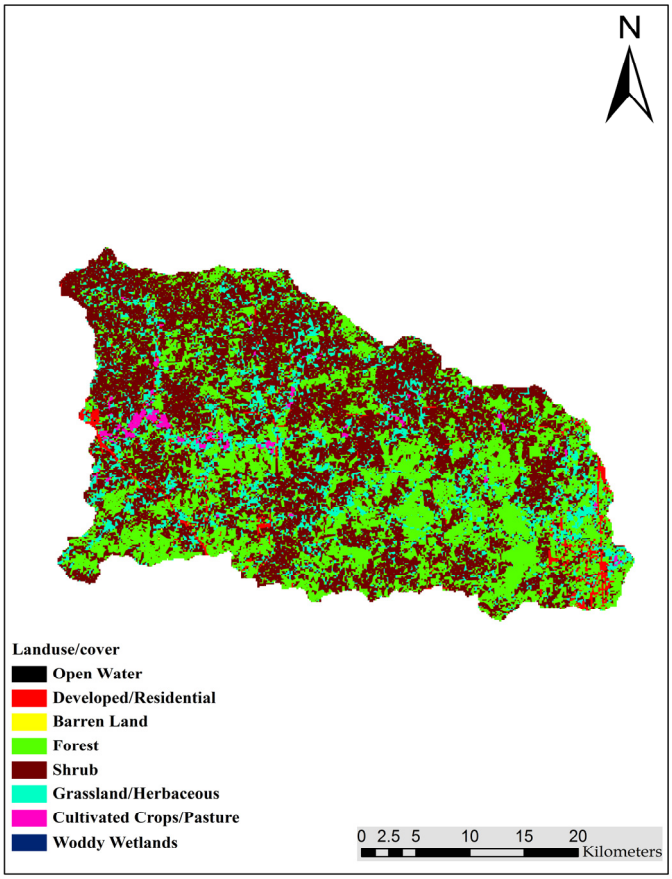

**Table 2.** Different soil types in the watershed.

| Soil type | % Soil in the basin |
|---|---|
| Clay loam | 45.93 |
| Silty clay | 9.64 |
| Clay | 25.54 |
| Very cobbly clay | 18.89 |

**Figure 5.** Soil types in the study area.

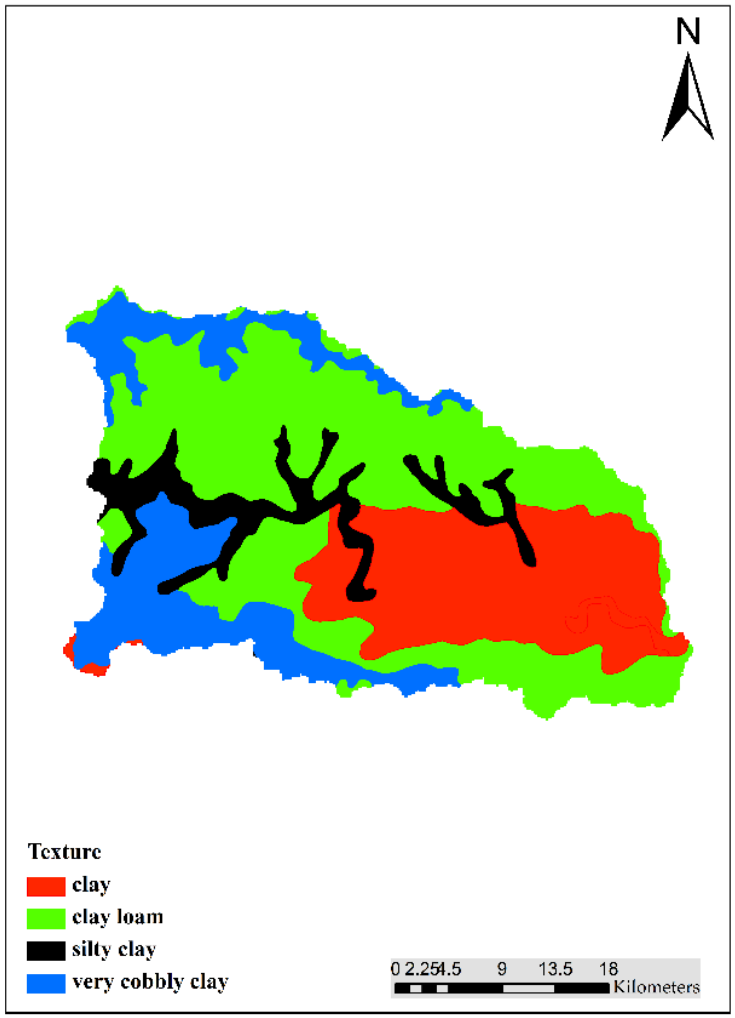


*5.2. Precipitation Products*

The rain gauge data was obtained from the Guadalupe Blanco River Authority (GBRA). There are eight rain gauges in the study area (seven in the watershed and one located adjacent to the watershed). There are other rain gauges in the area but are too far from the watershed to be considered. Figure 6 shows the location of the rain gauges. Due to the high quality of rain gauge data, the National Weather Service (MWS) use this rain gauge data to prepare NEXRAD MPE in this area. The 5-min rain gauge observations were aggregated into hourly accumulations and reformatted into a GSSHA precipitation file format [46]. The Inverse Distance interpolation method was used to construct rainfall maps from the rain gauge observations to facilitate comparison with the other rainfall products.

**Figure 6.** Location of rain gauges in the watershed.

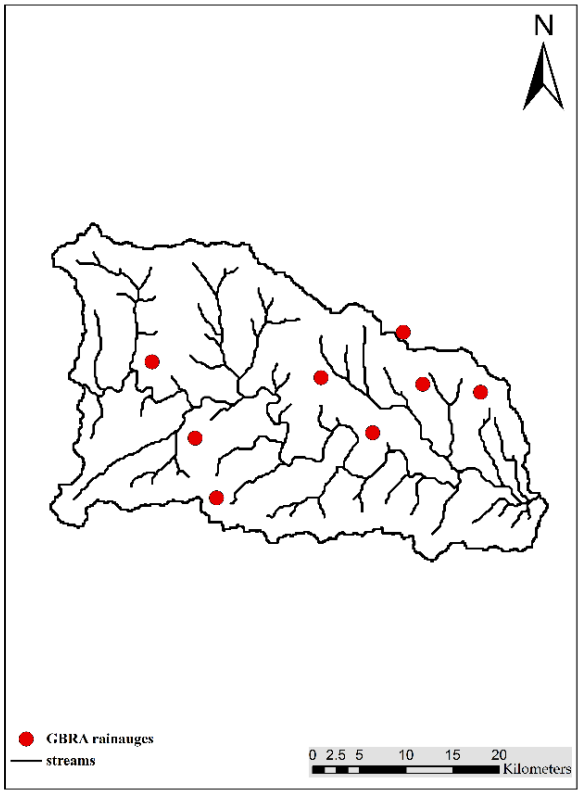


The NEXRAD MPE algorithm has replaced the Stage III algorithm [30]. The algorithm is based on merging different precipitation products such as rain gauge and satellite precipitation with NEXRAD raw data [47]. The NEXRAD MPE algorithm has proven to be superior to the Stage III algorithm in many areas [14]. The new algorithm consists of improved mean field bias correction and new local bias correction procedures. The NEXRAD MPE product used in this study is projected onto the Hydrologic Rainfall Analysis Project (HRAP) grid system. The Consortium of Universities for the Advancement of Hydrologic Science (CUASHI) Hydro Desktop tool was used to extract the NEXRAD MPE data. This tool has the capability to extract NEXRAD MPE data for the watershed coverage.

The TRMM 3B42V7 product used in this study has a spatial resolution of 0.25° × 0.25° and temporal resolution of three hours. This TRMM rainfall product, a 0.25 degree spatial resolution three hours temporal resolution precipitation product, is available between 50° S and 50° N latitude. The TRMM 3B42V7 precipitation product is produced in three stages and is bias-adjusted using rain gauge data. In the first stage, microwave precipitation estimates are calibrated and combined. In the second stage, IR precipitation estimates are calibrated and combined and in the third stage, the calibrated microwave and infra-red (IR) precipitation products are merged [7]. The TRMM 3B42V7 data were downloaded using NASA Mirador tool NASA website [48].

The PERSIANN products are prepared using on artificial neural networks to compute rainfall rates using merged infrared product from climate prediction center [8,49]. Sorooshian *et al.* [50] explained the detailed procedure of deriving PERSIANN products. The PERSIANN 0.25 degree spatial resolution and three-hour temporal resolution product has data coverage from 60° S to 60° N. The PERSIANN 0.25 degree product was downloaded from the PERSIANN website. The PERSIANN CCS-1hr and PERSIANN CCS-3hr products were produced based on cloud classification-based

neural networks. The new version of the CCS technique uses computer image processing and pattern recognition techniques to develop a patch-based cloud classification and rainfall estimation system based on satellite infrared images. While both versions of PERSIANN use neural networks, CCS [8] is a separate product, which was developed after PERSIANN [11,12]. PERSIANN uses a collection of microwave sensors to construct the relationship between infrared observation and precipitation rate. CCS is based on a cloud classification system and uses cloud segmentation while PERSIANN is pixel-based. PERSIANN CCS the identification and separation of individual patches of clouds and computes the gridded rainfall rates at 0.04° × 0.04° with 1- and 3-h temporal resolution [8,51]. The PERSIANN and CCS data were downloaded from PERSIANN website.

CMORPH is a global precipitation technique developed by NOAA's Climate Prediction Center [CPC] for real-time monitoring of global precipitation. CMORPH has the capability of providing precipitation estimates with 8 km spatial resolution and 30 min temporal resolution. This study used the CMORPH 0.25° spatial resolution and 3-h temporal resolution precipitation product. These data were downloaded from National Centers for Environmental Prediction (NCEP) CMORPH website. The CMORPH technique uses half-hourly geostationary satellite IR temperature fields and polar orbiting passive microwave (PMW) brightness temperature retrievals with irregular intervals. The morphing technique used to produce CMORPH precipitation estimates involves using the poor temporal resolution of PMW precipitation estimate data and interpolating its movement between retrieval periods.

### *5.3. AMSR-E Soil Moisture*

The Advanced Microwave Scanning Radiometer—Earth Observing System (AMSR-E) sensor provides measurements of precipitation rate, sea surface temperature, sea ice concentration, snow water equivalent, soil moisture, surface wetness, wind speed, atmospheric cloud water, and water vapor. In this study, level 3 soil moisture data of spatial resolution 25 km was used as the initial conditions for soil moisture. The AMSR-E satellite provides information on surface soil moisture twice a day (Descending, 1:30 am and ascending, 1:30 pm) Greenwich Mean Time (GMT) in the top 1 cm. Since the two storm events started at the beginning of the day, the AMSR-E descending data were selected as the initial conditions. The downloaded data have units of $g/cm^3$ and these units were converted into volumetric water content to use in the GSSHA model.

## 6. Model Setup

The GSSHA model developed for this study used a 150 m grid cell size and a time step of 20 s. Among the three available numerical methods, the ADE method was selected as an overland flow routing method, G&A with redistribution as the infiltration method, diffusive wave as the channel routing method, and the inverse distance method was used to distribute the spatially and temporally varied rainfall. By definition, fully distributed models use the parameters that can be accessed directly from the field. Therefore, the hydrologic parameters recommended by Gsshawiki [45] were used in this study as shown in Table 3. Those parameters were based on calibration in previous GSSHA modeling studies and some of them were assigned considering soil textural classification and land use data from published sources. Table 4 shows the initial soil moisture conditions used in the study

indicated by the volumetric water content, which is a model parameter for GSSHA. The initial soil moisture content was higher during the August 2007 event than during the July 2007 event. The Manning's roughness values used in this study are shown in Table 5. The hydrologic parameters shown in Tables 3 and 5 were used to drive the GSSHA model for different precipitation datasets.

**Table 3.** Soil hydrologic properties used in the study.

| Hydrologic parameter | Clay | Silty clay | Clay loam | Very cobbly clay |
|---|---|---|---|---|
| Hydraulic conductivity (cm/hr) | 0.06 | 0.1 | 0.2 | 0.15 |
| Capillary head (CM) | 31.63 | 29.22 | 20.88 | 31 |
| Porosity ($m^3/m^3$) | 0.385 | 0.423 | 0.39 | 0.385 |
| Pore distribution index (cm/cm) | 0.165 | 0.15 | 0.242 | 0.165 |
| Residual saturation ($m^3/m^3$) | 0.09 | 0.056 | 0.075 | 0.09 |

**Table 4.** Initial soil moisture conditions for both events.

| Initial moisture | Clay | Silty clay | Clay loam | Very cobbly clay |
|---|---|---|---|---|
| 7 July | 0.25 | 0.22 | 0.25 | 0.25 |
| 7 August | 0.28 | 0.25 | 0.27 | 0.27 |

**Table 5.** Manning's surface roughness values used in this study for different land covers.

| Land use | Manning's roughness |
|---|---|
| Open water | 0.01 |
| Developed areas | 0.15 |
| Barren land (ock/sand/clay) | 0.10 |
| Forest | 0.19 |
| Shrub/scrub | 0.18 |
| Grassland/herbaceous | 0.18 |
| Pasture/hay | 0.20 |
| Cultivated crops | 0.20 |
| Woody wetlands | 0.20 |

## 7. Performance Statistics

The simulation results driven by satellite, radar, and rain gauge precipitation products were evaluated by analyzing the error in peak discharge ($\varepsilon_p$), error in runoff volume ($\varepsilon_{rv}$), the Nash-Sutcliffe efficiency (*NSE*), and the square of the Pearson correlation coefficient (*R*). The following formulas were used to evaluate model performance.

$$\varepsilon_p(\%) = \frac{|Q_{po} - Q_{ps}|}{Q_{po}} \times 100 \quad (1)$$

$$\varepsilon_{rv}(\%) = \frac{|Q_o^v - Q_s^v|}{Q_o^v} \times 100 \quad (2)$$

$$NSE = 1 - \frac{[\sum_{t=1}^{N}(Q_o(t) - Q_s(t))^2]}{[\sum_{t=1}^{N}(Q_o(t) - \overline{Q_o})^2]} \quad (3)$$

$$R = \sqrt{\frac{\left(\sum_{t=1}^{N}(Q_s(t) - \overline{Q_s})\,(Q_o(t) - \overline{Q_o})\right)^2}{\sum_{t=1}^{N}(Q_s(t) - \overline{Q_s})^2 \sum_{t=1}^{N}(Q_o(t) - \overline{Q_o})^2}} \quad (4)$$

where, $Q_{po}$ and $Q_{ps}$ are the observed and simulated peak discharges; $Q_o^v$ and $Q_s^v Q_o^v$ and $Q_s^v$ are the observed and simulated runoff volumes; $Q_s(t)$ and $Q_o(t)$ refers to the model simulated and observed discharge, respectively; $N$ is the total number of discharge ordinates used in the comparison; $\overline{Q_o}$ and $\overline{Q_s}$ are observed and simulated mean discharge values, respectively.

## 8. Results and Discussion

### *8.1. Differences among Precipitation Products*

All of the precipitation products used in this study had different spatial and temporal resolutions. NEXRAD MPE and PERSIANN CCS-1hr had the finest spatial and temporal resolutions of 0.04 degree and 1 h, respectively. PERSIANN 0.25 degree, CMORPH, and TRMM 3B42V7 had the coarsest spatial and temporal resolutions of approximately 25 km and 3 h, respectively. Figures 7–10 show the basin average precipitation comparison for the July 2007 and August 2007 events respectively.

**Figure 7.** Basin average precipitation comparison for the July 2007 storm event.

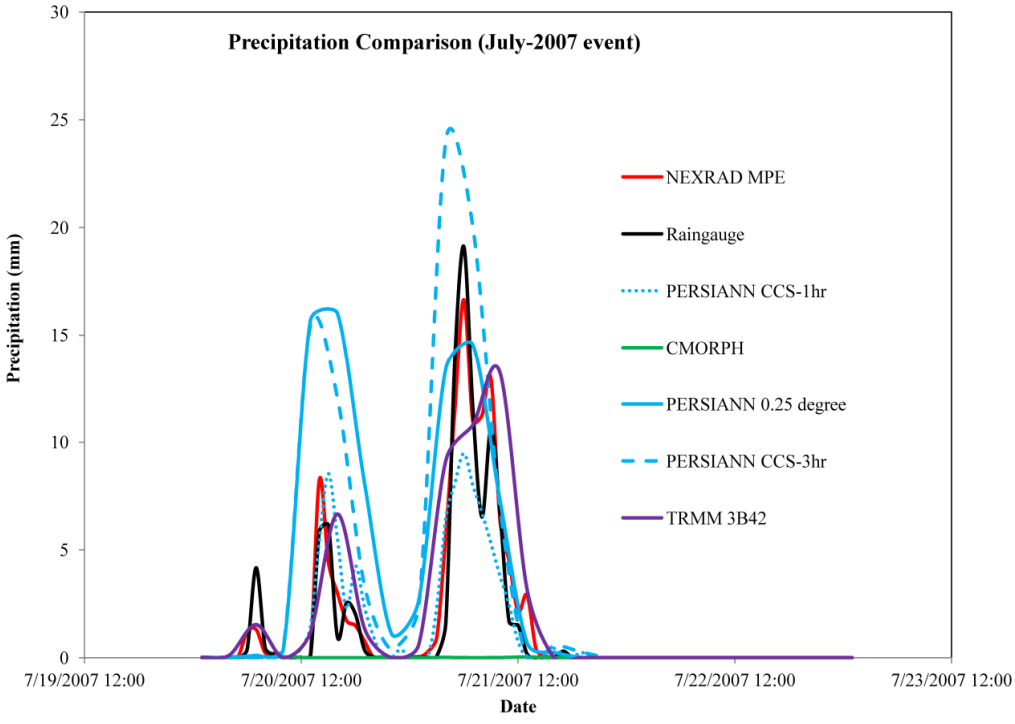


All of the precipitation products were able to reproduce the shape and size of the precipitation patterns observed by the rain gauges for the July 2007 event. The time series of the NEXRAD MPE and rain gauge precipitation estimates matched very well with a correlation coefficient $R = 0.98$. There were significant differences among the PERSIANN precipitation products. However, all of these products were able to reproduce the shape and size of the rainfall patterns of the NEXRAD MPE and rain gauge rainfall. The PERSIANN CCS-3hr product significantly overestimated the rainfall peaks,

PERSIANN CCS-1hr significantly underestimated the second peak, and the PERSIANN 0.25 degree product overestimated the first peak and underestimated the second peak (Figure 7). However, strong correlations existed between NEXRAD MPE *vs.* PERSIANN CCS-1hr and rain gauge *vs.* PERSIANN CCS 1-hr with *R* values of =0.94 and 0.92, respectively. The bias-adjusted TRMM 3B42V7 was able to reproduce all of the rainfall peaks except the biggest peak (underestimated). CMORPH significantly underestimated the rainfall and showed almost zero rainfall (Figure 7). The PERSIANN 0.25 degree and PERSIANN CCS 3-hr products significantly overestimated the rainfall (Table 6).

**Figure 8.** Average precipitation distribution for different precipitation products for the July 2007 event: (**a**) radar; (**b**) raingauges; (**c**) PERSIANN CCS-1hr; (**d**) PERSIANN CCS-3hr; (**e**) TRMM 3B42V7; (**f**) and PERSIANN 0.25 degree.

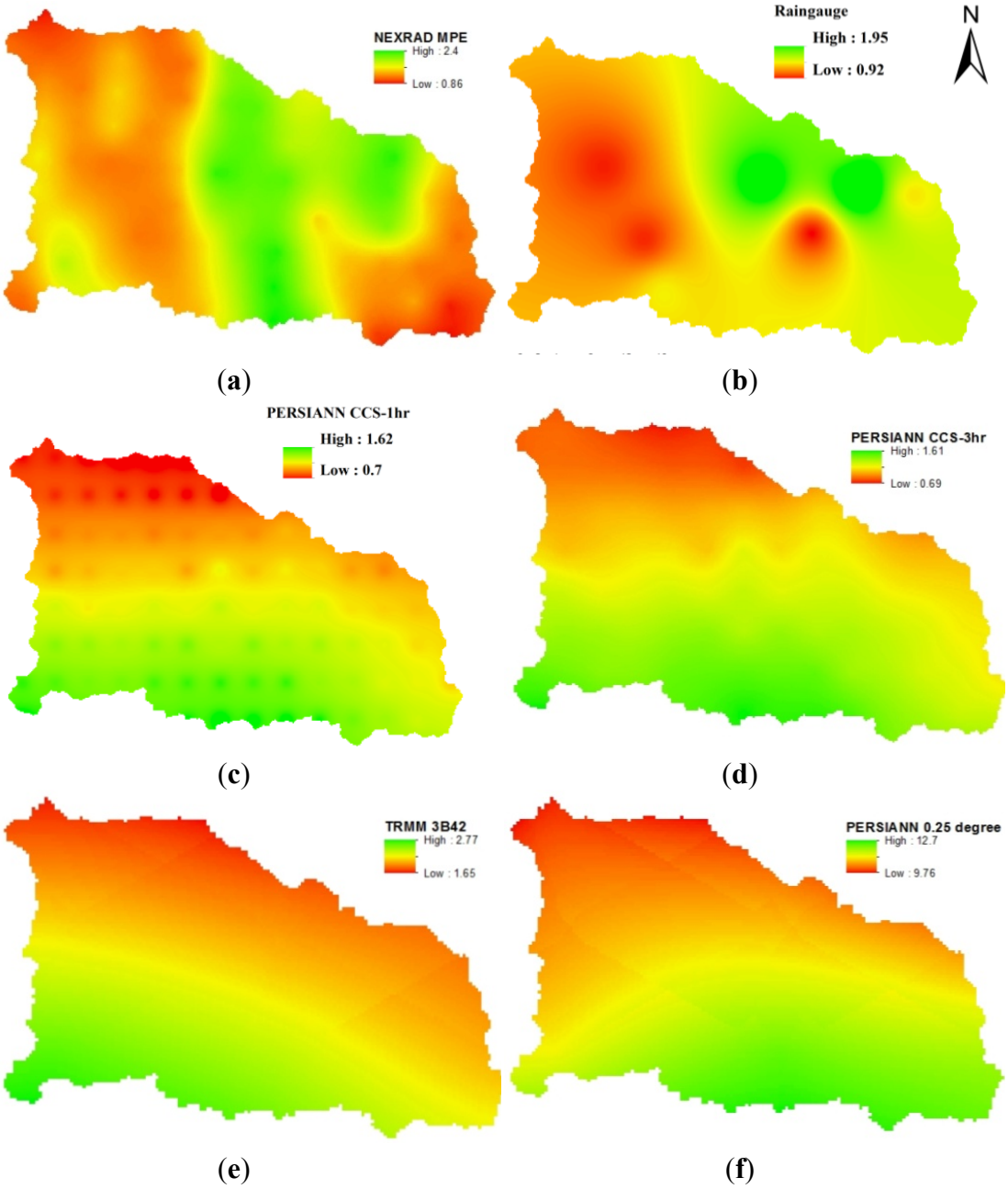

**Figure 9.** Basin average precipitation comparison for the August 2007 storm event.

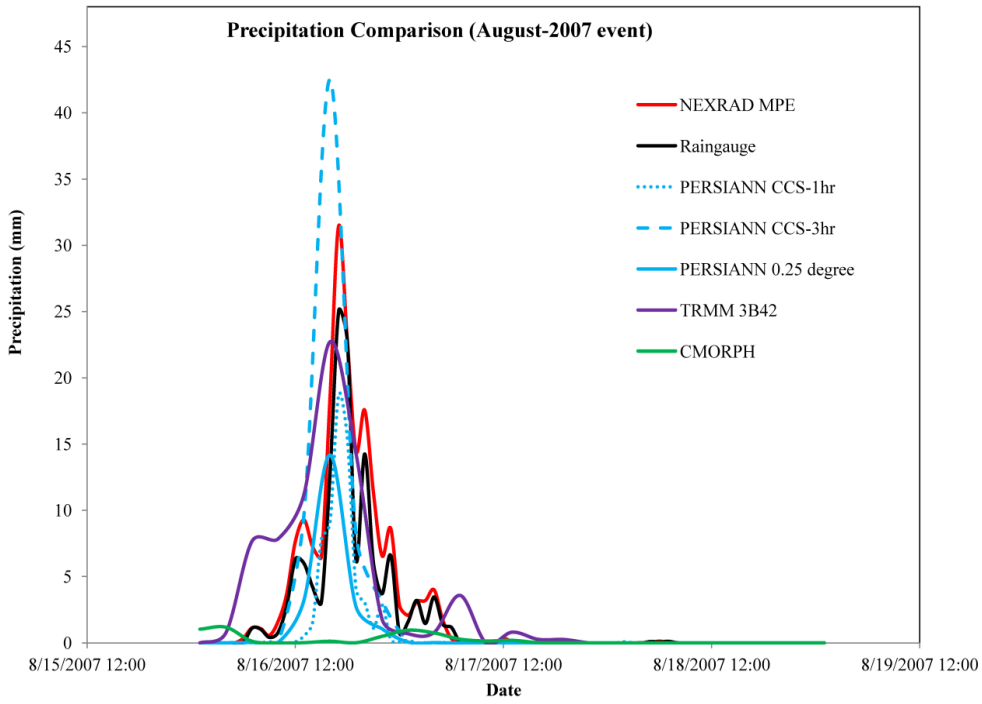


**Figure 10.** Average precipitation distribution for different precipitation products for the August 2007 event: (**a**) radar; (**b**) raingauges; (**c**) PERSIANN CCS-1hr; (**d**) PERSIANN CCS-3hr; (**e**) TRMM 3B42V7; (**f**) PERSIANN 0.25 degree.

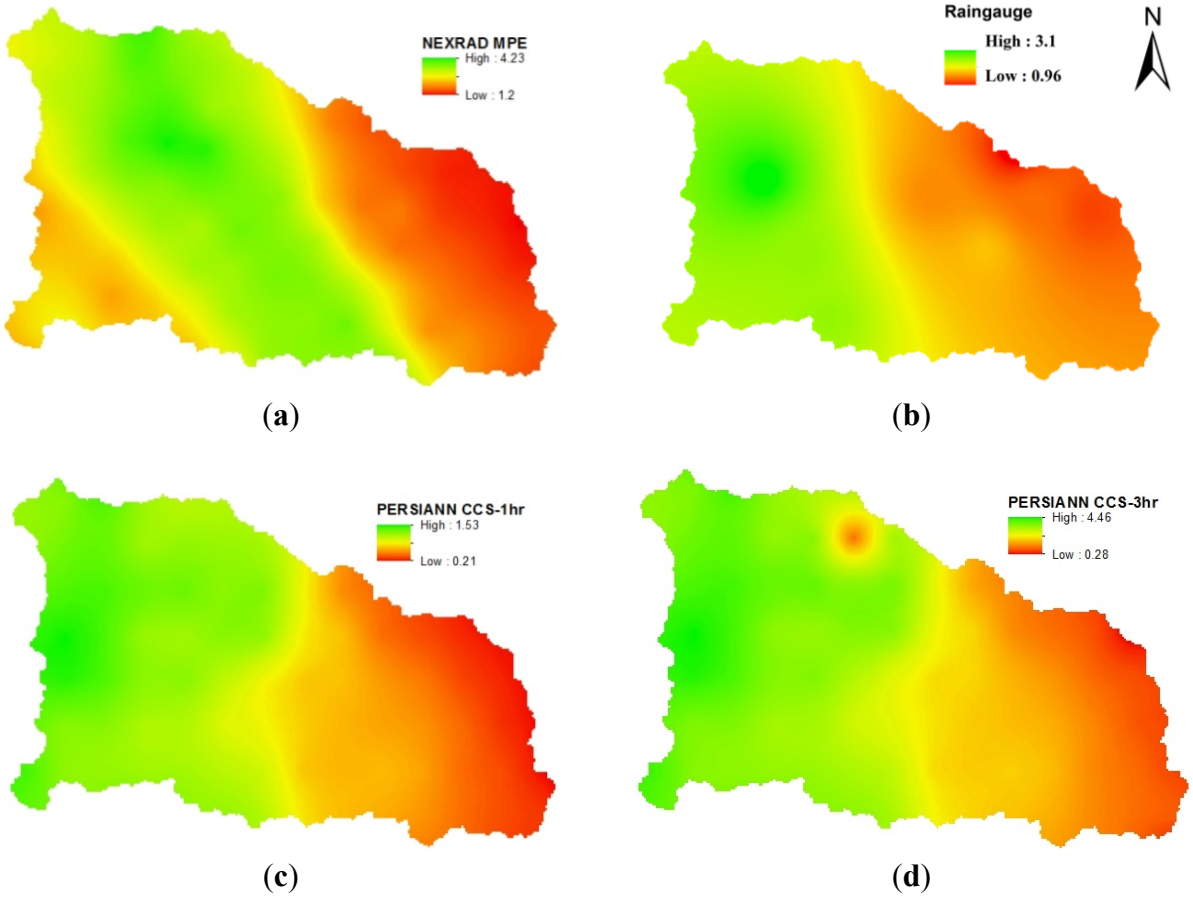

**Figure 10.** *Cont.*

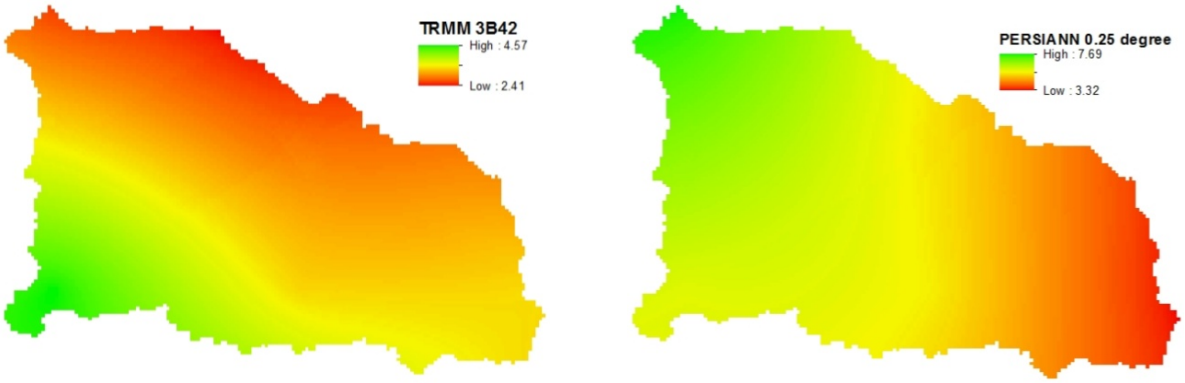


**(e)** **(f)**

**Table 6.** Volume of rainfall amounts over the study area.

| Precipitation product | Volume of rainfall [$m^3$] | |
|---|---|---|
| | 7-July | 7-August |
| NEXRAD MPE | $1.4 \times 10^8$ | $2.5 \times 10^8$ |
| Rain gauge | $1.1 \times 10^8$ | $1.8 \times 10^8$ |
| PERSIANN 0.25 degree | $3.3 \times 10^8$ | $1.6 \times 10^8$ |
| PERSIANN CCS-1hr | $1.1 \times 10^8$ | $8.3 \times 10^7$ |
| PERSIANN CCS-3hr | $3.2 \times 10^8$ | $2.4 \times 10^8$ |
| TRMM 3B42V7 | $2.0 \times 10^8$ | $3.0 \times 10^8$ |
| CMORPH | $5.5 \times 10^5$ | $1.7 \times 10^7$ |

Figure 8 shows the spatial distribution of average precipitation for the July 2007 storm event. The PERSIANN precipitation products showed that maximum rainfall intensities were recorded in the southwestern and southeastern portions of the watershed. However, the intensities of the PERSIANN precipitation products varied significantly. TRMM 3B42V7 map showed that the highest rainfall intensities were in the southwestern portion of the watershed, which was around 2.67 mm/h. The NEXRAD MPE spatial distribution indicated that the middle portion of the basin received the highest intensity of rainfall, but the rain gauge network observations showed that the highest rainfall amounts were in the northeastern portion of the watershed (Figure 8).

The average precipitation comparison for the August 2007 event showed that all precipitation datasets were able to reproduce the patterns of ground measured precipitation and NEXRAD MPE. NEXRAD MPE reproduced all of observed the peaks and rainfall volumes recorded by rain gauge network achieving the highest correlation between observed and simulated flow time series (0.99). TRMM 3B42V7 was able to reproduce the peak but did not capture variations in rainfall. PERSIANN CCS-3hr overestimated the rainfall peak by 70% with respect to the rain gauge rainfall peak. The PERSIANN 0.25 degree and PERSIANN CCS-1hr products underestimated the rainfall peaks by 43% and 25%, respectively. None of the PERSIANN precipitation products captured the temporal variability of precipitation patterns later in the storm event. However, the correlation between PERSIANN CCS-1hr and rain gauge was 0.95 (Figure 9). The CMORPH basin average precipitation was significantly low when compared to the other precipitation products. NEXRAD MPE was the only dataset that captured the temporal patterns of rainfall that were recorded by rain gauge (Figure 9).

The spatial distribution of the average precipitation over the study area for the August 2007 storm event, based on observations by the rain gauge network, showed that upstream portion received significant amounts of rainfall (Figure 10). The NEXRAD MPE recorded the highest rainfall intensities along a strip that extended from the northwestern to the southeastern part of the watershed. All of the PERSIANN products showed the highest rainfall recorded in the northwestern and southwestern portions of the watershed, but the PERSIANN 0.25 degree product showed that the highest rainfall intensities were around the upper northwestern portion of the watershed. The TRMM 3B42V7 average precipitation spatial distributions indicated that the highest rainfall intensities were in lower southwestern part of the watershed (Figure 10).

### *8.2. Hydrologic Model Simulations*

The GSSHA model was run for the July 2007 and August 2007 storm events. The same set of hydrologic parameters was used for both events. The duration of both storm events was three days. The July 2007 storm event started at 20 July 2007 01:00 CDT and ended at 23 July 2007 01:00 CDT. The August 2007 storm event started at 16 August 2007 01:00 CDT and ended at 19 August 2007 01:00 CDT. Since CMORPH showed approximately zero rainfall in both events, the CMORPH precipitation was not considered during streamflow simulations. The simulated streamflows were recorded at 15-min time intervals to match the USGS observed streamflow data.

All of the simulated streamflows driven by different precipitation products were able to reproduce the shape of the observed hydrograph (Figure 11). Among all of the precipitation products used, the NEXRAD MPE simulated flows best matched the observed streamflows with a high *NSE* of 0.93 and an *R* value of 0.99. The NEXRAD MPE simulated streamflows overestimated the peak discharge and runoff volume by 3.66% and 13.26%, respectively. There were significant differences among the PERSIANN product simulated streamflows. The PERSIANN 0.25 degree and PERSIANN CCS-3hr products significantly overestimated the peak and runoff volumes. However, the PERSIANN 0.25 degree and the PERSIANN CCS-3hr simulated streamflows were highly correlated with the observed streamflows with *R* values of 0.75 and 0.84, respectively (Table 7, Figure 11). The PERSIANN CCS-1hr simulated streamflows significantly underestimated the peak and runoff volumes with low *NSE* and *R* values. Negative *NSE* values existed between PERSIANN 0.25 degree and PERSIANN CCS-3hr simulated streamflows to the observed streamflows. The rain gauge simulated streamflows underestimated the peak and runoff volumes by 41.43% and 19.54%, respectively. However, the resulted hydrograph was able to reproduce the observed streamflow patterns with high *NSE* and *R* values. The TRMM 3B42V7 simulated streamflows significantly overestimated the peak and runoff volumes by 47.85% and 72%, respectively, with negative *NSE* and strong *R* values.

For the August 2007 storm event, the NEXRAD MPE simulated streamflows overestimated the peak and runoff volumes by 81.62% and 24.63%, respectively, with low *NSE* and high *R* values. The NEXRAD MPE and the TRMM 3B42V7 simulated streamflows matched perfectly by overestimating the peak and runoff volumes (Figure 12, Table 7). As expected, there were significant differences among the simulated streamflows driven by the PERSIANN precipitation products. However, the PERSIANN 0.25 degree simulated hydrograph matched closely the observed hydrograph with high

*NSE* (0.85) and *R* (0.99) values. The rain gauge simulated streamflows were able to reproduce the peak discharge and runoff volume with low errors and high *NSE* (0.89) and *R* (0.97) values.

**Figure 11.** Comparison of observed and simulated streamflow for the July 2007 storm event.

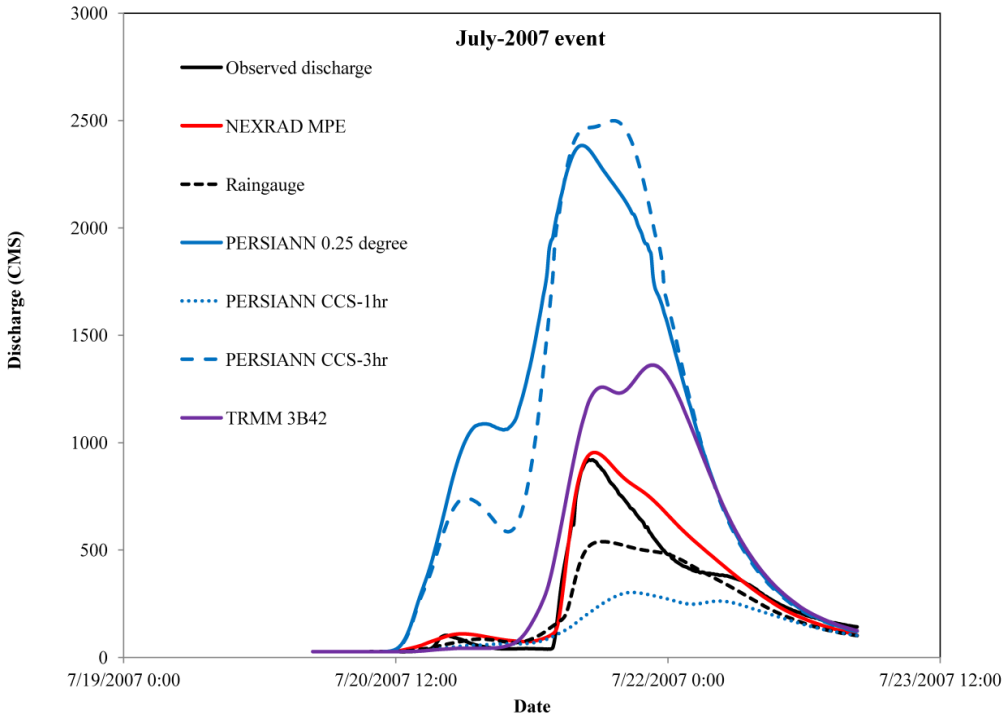


**Figure 12.** Comparison of observed and simulated streamflow for the August 2007 storm event.

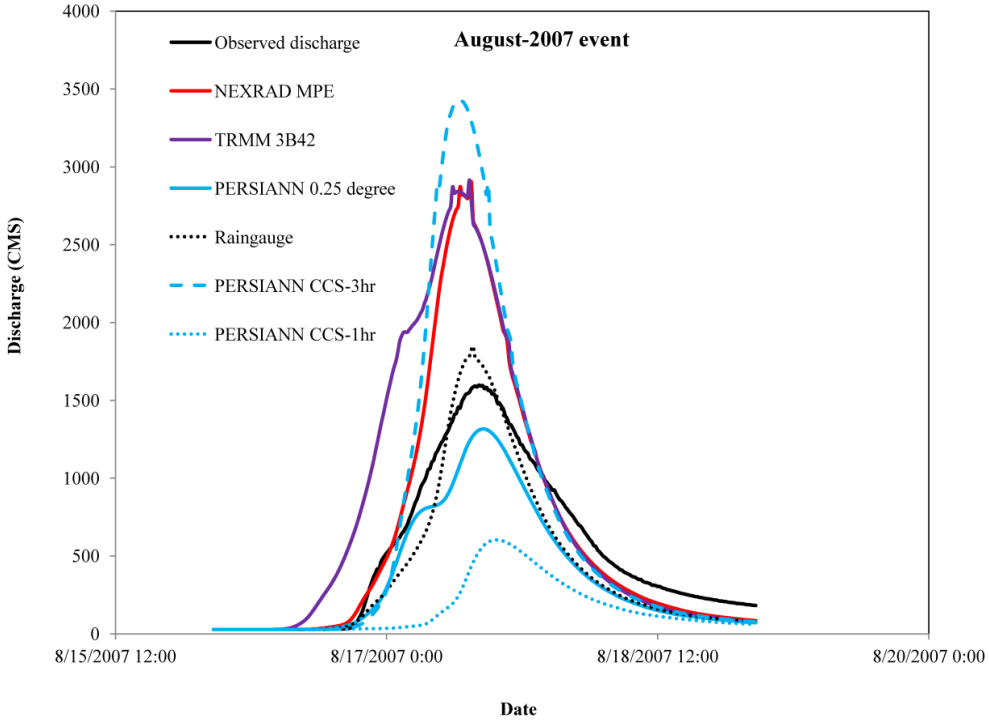

**Table 7.** Performance evaluation of simulated streamflows driven by different precipitation products (+ve and −ve signs represent the over and underestimation, respectively).

| Precipitation product | $\varepsilon_p$ [%] | | $\varepsilon_{rv}$ [%] | | *NSE* | | *R* | |
|---|---|---|---|---|---|---|---|---|
| | 7 July | 7 August | 7 July | 7 August | 7 July | 7 August | 7 July | 7 August |
| NEXRAD | 3.66 | 81.62 | 13.26 | 24.63 | 0.93 | 0.35 | 0.99 | 0.95 |
| PERSIANN CCS-3hr | 171.49 | 114.74 | 229.33 | 36.47 | −10.00 | −0.53 | 0.84 | 0.92 |
| PERSIANN CCS-1hr | −67.19 | −62.23 | −46.92 | −69.58 | 0.27 | −0.09 | 0.84 | 0.83 |
| TRMM 3B42V7 | 47.85 | 82.50 | 72.12 | 53.76 | −0.49 | −0.37 | 0.92 | 0.89 |
| Rain gauges | −41.43 | 15.49 | −19.54 | −19.00 | 0.79 | 0.89 | 0.94 | 0.97 |
| PERSIANN 0.25degree | 159.07 | −17.59 | 244.10 | −28.76 | −10.40 | 0.85 | 0.75 | 0.99 |

### *8.3. Infiltration*

For the July 2007 storm event, the spatial distributions of cumulative infiltration derived from all precipitation products showed a similar pattern except for minor differences (Figure 13). Cumulative infiltration was lower in clay soils because of the low hydraulic conductivity. The NEXRAD MPE and the rain gauge derived cumulative infiltration distributions showed very similar cumulative infiltration patterns throughout the watershed. The cumulative infiltration rates were higher in the watershed for the PERSIANN 0.25 degree, PERSIANN CCS-3hr, and the TRMM 3B42V7 rainfall datasets. However, the infiltration rates for the TRMM 3B42V7 data set were lower than for the PERSIANN 0.25 degree and the PERSIANN CCS-3hr rainfall data sets. For the PERSIANN CCS-1 hr rainfall, cumulative infiltration rates were higher in the middle and downstream portion of the watershed. Table 8 shows the rainfall volumes and percentages of rainfall infiltrated into the ground for both events. Higher rainfall volumes can result in lower infiltration depending on the spatiotemporal distribution of the rainfall as can be seen in Figure 13 and *vice versa*. For the July 2007 event, the rainfall volumes for the PERSIANN 0.25 degree and the PERSIANN CCS-3 hr were $3.3 \times 10^8$ and $3.2 \times 10^8$ cubic meters, respectively, while the percentages of infiltrated water were 30.68% and 30.6%. The percentage of rainfall volume that infiltrated into the basin for NEXRAD MPE, rain gauge, and PERSIANN CCS-1hr were 47.48%, 54.86%, and 68.6%, while their rainfall volumes ranged from $1.1 \times 10^8$ to $1.4 \times 10^8$ cubic meters.

For the August 2007 storm event, the NEXRAD MPE and rain gauge rainfall showed a similar pattern in their cumulative spatial distributions. Both rainfall datasets showed that the cumulative infiltrations were higher in the northwestern portion of the basin. The cumulative infiltration rates were very low in the downstream portion of the basin and higher in the upstream portion for the PERSIANN CCS-1hr rainfall dataset. However, the PERSIANN 0.25 degree distribution showed the highest cumulative infiltration throughout the basin, while the PERSIANN CCS-3hr showed the most modest cumulative infiltration (Figure 14). The TRMM 3B42V7 cumulative infiltration values were higher among all of the cumulative infiltration distributions. These infiltration rates were higher in the middle and downstream portions and lower in the upstream portion of the watershed. As discussed above, the infiltration fraction amounts were lower for high rainfall volumes and higher for lower rainfall volumes (Table 8).

**Figure 13.** Spatial distribution of cumulative infiltration depths (m) driven by different precipitation products for the July 2007 event: (**a**) radar; (**b**) raingauges; (**c**) TRMM 3B42V7; (**d**) PERSIANN 0.25 degree; (**e**) PERSIANN CCS-3hr; (**f**) PERSIANN CCS-1hr.

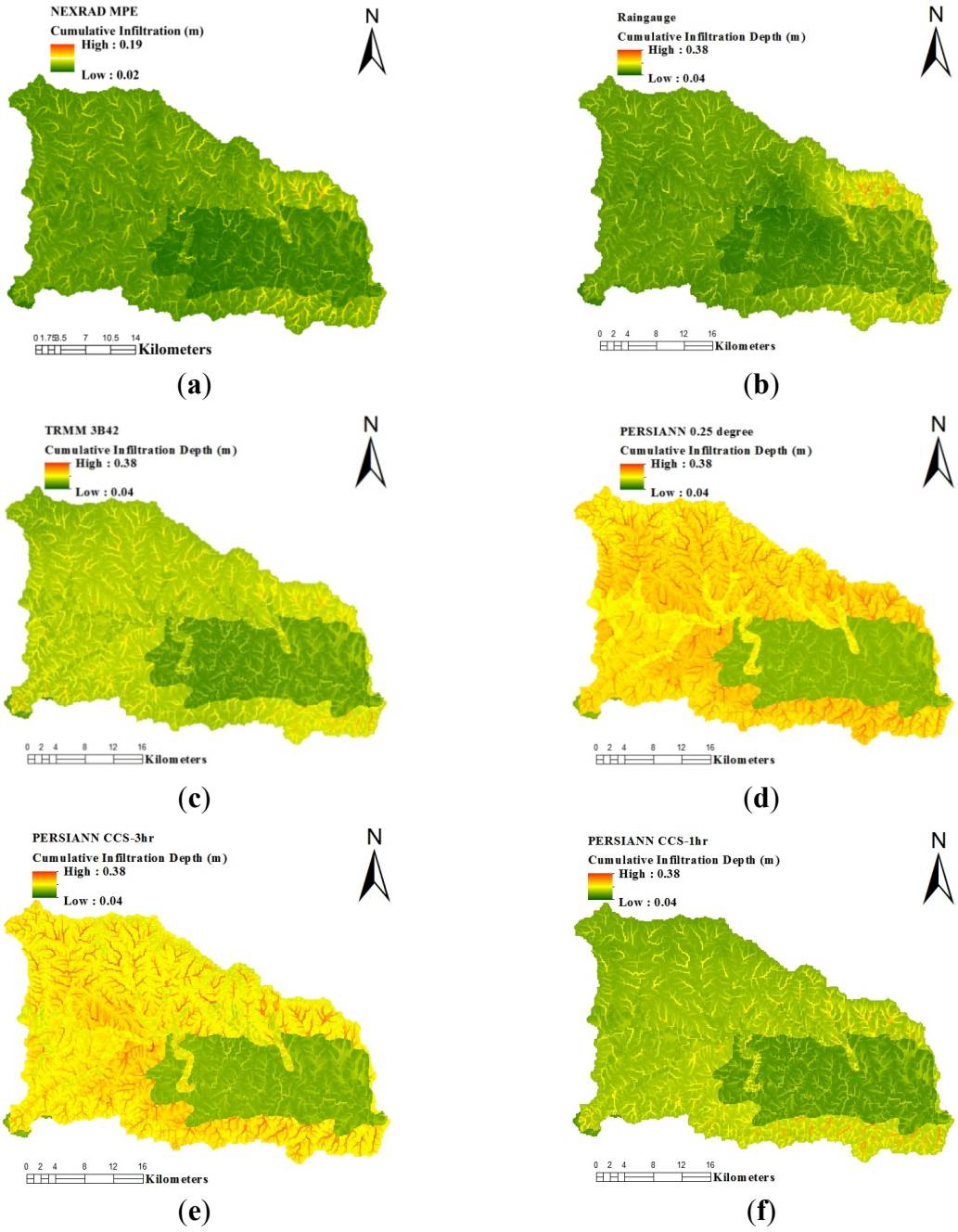


**Table 8.** Percentage of rainfall volumes infiltrated into the ground and volume of rainfall amounts for the two events.

| Precipitation product | % of rainfall infiltrated into the ground | | Volume of rainfall | |
|---|---|---|---|---|
| | 7-July | 7-August | 7-July | 7-August |
| NEXRAD MPE | 47.48 | 31.90 | $1.4 \times 10^8$ | $2.5 \times 10^8$ |
| Rain gauges | 54.86 | 41.30 | $1.1 \times 10^8$ | $1.8 \times 10^8$ |
| PERSIANN 0.25 degree | 30.68 | 42.72 | $3.3 \times 10^8$ | $1.6 \times 10^8$ |
| PERSIANN CCS-1hr | 68.60 | 55.51 | $1.1 \times 10^8$ | $8.3 \times 10^7$ |
| PERSIANN CCS-3hr | 30.66 | 24.84 | $3.2 \times 10^8$ | $2.4 \times 10^8$ |
| TRMM 3B42V7 | 41.15 | 30.52 | $2.0 \times 10^8$ | $3.0 \times 10^8$ |

**Figure 14.** Spatial distribution of cumulative infiltration depths (m) driven by different precipitation products for the August 2007 event: (**a**) radar; (**b**) raingauges; (**c**) TRMM 3B42V7; (**d**) PERSIANN 0.25 degree; (**e**) PERSIANN CCS-3hr; (**f**) PERSIANN CCS-1hr.

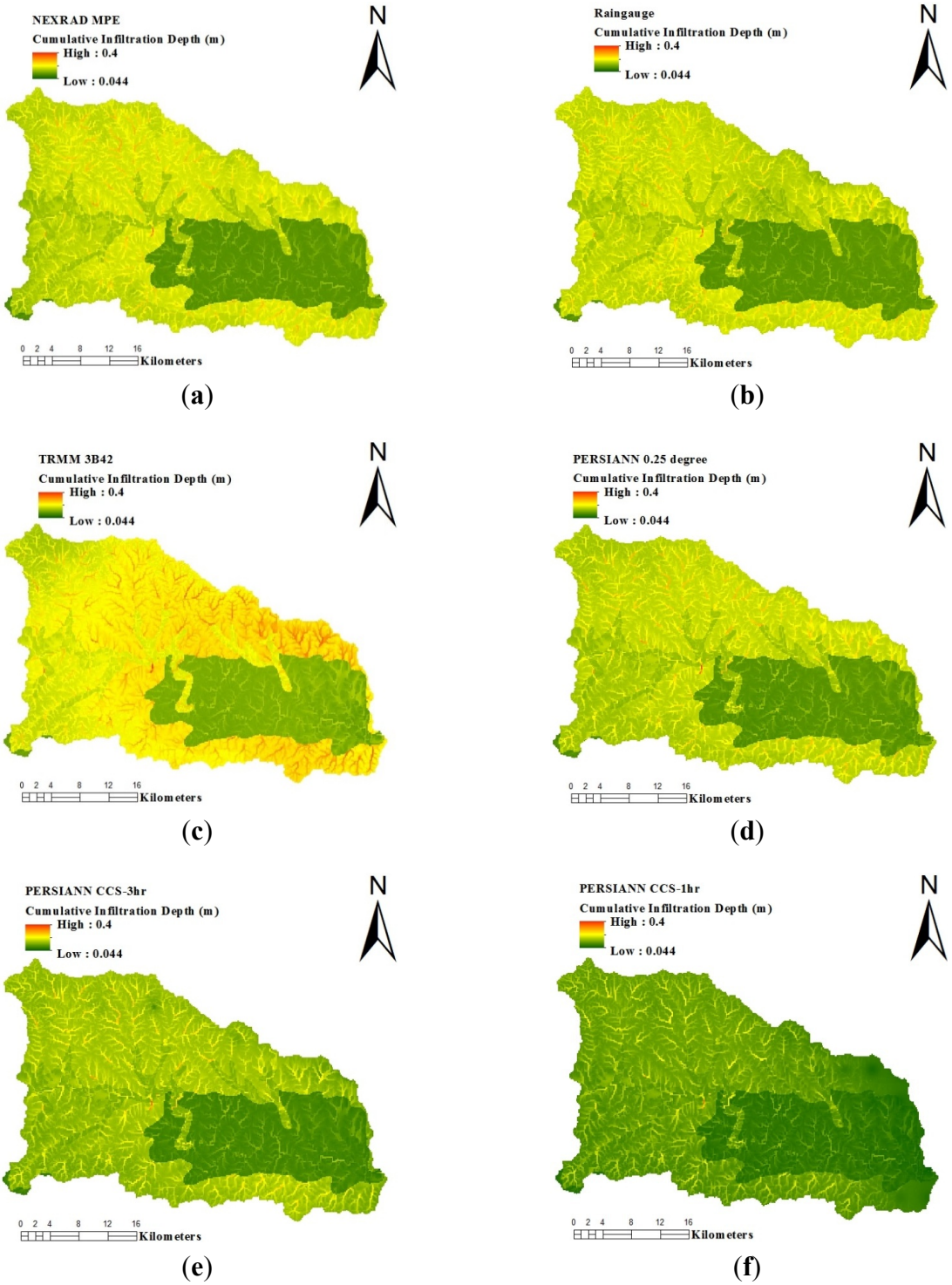


## 9. Conclusions

This study evaluated the PERSIANN, TRMM 3B42V7, CMORPH, rain gauge, and NEXRAD MPE precipitation products as an input to the physically-based, distributed-parameter hydrologic model GSSHA over the Guadalupe River basin below Comfort and above Canyon Lake. The July and

August 2007 events were used to evaluate the capability of each precipitation product in estimating streamflows. The model simulated streamflows were reported at a 15-min temporal scale to match with the USGS IDA observed hydrograph. In general, the model was able to predict streamflows driven by all precipitation products (except for CMORPH) reasonably well in terms of reproducing the shape.

The basin average precipitation comparison results showed that NEXRAD MPE estimates were the closest to rain gauge rainfall observations for both events although it showed an overestimation of the rainfall peak. There were significant differences among the three PERSIANN products. The PERSIANN CCS-3hr precipitation product significantly overestimated the rainfall peak and rainfall volume for both events. The coarse resolution PERSIANN product overestimated the rainfall volume and underestimated the peak and rainfall volumes in the July 2007 and August 2007 events, respectively (Figures 7 and 9). PERSIANN CCS-1hr underestimated the peak and rainfall volumes in both events. This suggests that bias correction procedures may have to be applied before using the products as inputs to a hydrologic model. The bias-adjusted TRMM 3B42V7 product was able to reasonable match the peak and rainfall volumes for both events. These results agree, in general, with results from other studies (e.g., [7,44]). However, for both events, CMORPH significantly underestimated the rainfall, which is contrary to other studies showing that CMORPH products performed well in hydrometeorological applications (e.g., [27,38,52,53]). Among all of the remote sensing precipitation products, the NEXRAD MPE basin average precipitation best matched the rain gauge basin average precipitation. The TRMM 3B42V7 product showed better precipitation comparison with rain gauge precipitation among all satellite precipitation products.

NEXRAD MPE proved to be the best precipitation dataset to model streamflows for the July 2007 storm event. However, during the August 2007 event, it overestimated the peak and runoff volumes. Due to the significant biases in the PERSIANN precipitation products, the PERSIANN CCS-3hr product significantly overestimated the peak discharge and runoff volumes in both events. However, the PERSIANN CCS-1hr product underestimated the peak discharge and runoff volumes in both events. The coarse resolution precipitation product (PERSIANN 0.25 degree) overestimated the peak discharge and runoff volumes for the July 2007 event and underestimated them for the August 2007 event. For both events, the TRMM 3B42V7 product overestimated the simulated peak discharge and runoff volumes. Due to the low density of the rain gauge network, it underestimated the peak discharge and runoff volume during the July 2007 event and overestimated the peak discharge in the August 2007 event.

In summary, NEXRAD MPE was the best precipitation dataset among all precipitation datasets as it provided high *NSE* and *R* values compared to rain gauge precipitation. However, satellite products are able to capture the general patterns and are viable alternatives for precipitation estimation in remote regions where rain gauge or ground radars are sparse or non-existent. Among all the satellite precipitation products, TRMM 3B42V7 produced simulated streamflows that are reasonably well in both events. The infiltration amounts showed that the type of storm event has a significant effect on infiltration. Satellite precipitation products may need vigorous validation and comparison with ground truth before being used as input for hydrologic simulations over catchment of the size used in this study or smaller. More studies on the application of satellites in hydrologic simulations are needed and the results of this study should not be generalized. The aim of this study was to compare the hydrologic simulations forced by different rainfall products without calibration of the hydrologic to a specific

product. Other studies that tested recalibration of a hydrologic to a certain precipitation product (e.g., satellite rainfall) can lead to improvement in the hydrologic simulations forced by that specific product (e.g., [52]).

**Acknowledgments**

This study was supported in part by NASA Grant (NNX11AE42G).

**Author Contributions**

This paper presents part of Singaiah Chintalapudi Ph.D. study research. Singaiah Chintalapudi Ph.D. study was advised by Hatim O. Sharif and Hongjie Xie who guided his research and contributed significantly to preparing the manuscript for publication. Hongjie Xie designed the remote sensing portion of the study and Hatim O. Sharif designed the hydrologic modeling portion with input from Singaiah Chintalapudi who downloaded the remote sensing products and prepared and performed the hydrologic model simulations. Singaiah Chintalapudi conducted post-analysis of the model outputs and prepared the first draft. Hongjie Xie and Hatim O. Sharif reviewed and revised the remote sensing and hydrologic modeling portions of the manuscript. Hatim O. Sharif did the final overall proof reading of the manuscript.

**Conflicts of Interest**

The authors declare no conflict of interest.

**References**

1. Ebert, E.E.; Janowiak, J.E.; Kidd, C. Comparison of near-real-time precipitation estimates from satellite observations and numerical models. *Bull. Am. Meteorol. Soc.* **2007**, *88*, 47–64.
2. Meskele, T.; Moradkhani, H. Impacts of different rainfall estimates on hydrologic simulation and satellite rainfall retrieval error propagation. Presented at World Environmental and Water Resources Congress 2009, Kansas City, MO, USA, 17–21 May 2009; American Society of Civil Engineers: Kansas, MO, USA, 2009.
3. Tsintikidis, D.; Georgakakos, K.P.; Sperfslage, J.A.; Smith, D.E.; Carpenter, T.M. Precipitation uncertainty and rain gauge network design within Folsom Lake watershed. *J. Hydrol. Eng.* **2002**, *7*, 175–184.
4. Chintalapudi, S.; Sharif, H.O.; Yeggina, S.; Elhassan, A. Physically-based, hydrologic model results based on three precipitation products. *J. Am. Water Resour. Assoc. JAWRA* **2012**, *48*, 1191–1203.
5. Sharif, H.O.; Yates, D.; Roberts, R.; Mueller, C. The use of an automated now-casting system to forecast flash floods in an urban watershed. *J. Hydrometeorol.* **2006**, *7*, 190–202.
6. Curtis, S.; Crawford, T.W.; Lecce, S.A. A comparison of TRMM to other basin-scale estimates of rainfall during the 1999 Hurricane Floyd flood. *Nat. Hazards* **2007**, *43*, 187–198.

7. Huffman, G.J.; Adler, R.F.; Bolvin, D.T.; Gu, G.J.; Nelkin, E.J.; Bowman, K.P.; Hong, Y.; Stocker, E.F.; Wolff, D.B. The TRMM multisatellite precipitation analysis (TMPA): Quasi-global, multiyear, combined-sensor precipitation estimates at fine scales. *J. Hydrometeorol.* **2007**, *8*, 38–55.
8. Hong, Y.; Hsu, K.L.; Sorooshian, S.; Gao, X.G. Precipitation estimation from remotely sensed imagery using an artificial neural network cloud classification system. *J. Appl. Meteorol.* **2004**, *43*, 1834–1852.
9. Behrangi, A.; Khakbaz, B.; Jaw, T.C.; AghaKouchak, A.; Hsu, K.; Sorooshian, S. Hydrologic evaluation of satellite precipitation products over a mid-size basin. *J. Hydrol.* **2011**, *397*, 225–237.
10. Krakauer, N.; Pradhanang, S.; Lakhankar, T.; Jha, A. Evaluating satellite products for precipitation estimation in mountain regions: A case study for nepal. *Remote Sens.* **2013**, *5*, 4107–4123.
11. Thiemig, V.; Rojas, R.; Zambrano-Bigiarini, M.; de Roo, A. Hydrological evaluation of satellite-based rainfall estimates over the Volta and Baro-Akobo Basin. *J. Hydrol.* **2013**, *499*, 324–338.
12. Hsu, K.L.; Gao, X.G.; Sorooshian, S.; Gupta, H.V. Precipitation estimation from remotely sensed information using artificial neural networks. *J. Appl. Meteorol.* **1997**, *36*, 1176–1190.
13. Joyce, R.J.; Janowiak, J.E.; Arkin, P.A.; Xie, P. CMORPH: A method that produces global precipitation estimates from passive microwave and infrared data at high spatial and temporal resolution. *J. Hydrometeorol.* **2004**, *5*, 487–503.
14. Stisen, S.; Sandholt, I. Evaluation of remote-sensing-based rainfall products through predictive capability in hydrologic runoff modelling. *Hydrol. Process*. **2010**, *24*, 879–891.
15. Xie, H.; Xiaobing, Z.; Vivoni, E.R.; Hendrickx, J.M.H.; Small, E.E. GIS-based NEXRAD Stage III precipitation database: Automated approaches for data processing and visualization. *Comput. Geosci.* **2005**, *31*, 65–76.
16. Collier, C.G. Accuracy of rainfall estimates by radar, part II: Comparison with rain gauge network. *J. Hydrol.* **1986**, *83*, 225–235.
17. Sharif, H.O.; Chintalapudi, S.; Elhassan, A.; Xie, H.; Zeitler, J. Physically-based hydrologic modeling of the 2002 floods in San Antonio, Texas. *J. Hydrol. Eng.* **2013**, *18*, 228–236.
18. Sharif, H.O.; Hassan, A.A.; Bin-Shafique, S.; Xie, H.; Zeitler, J. Hydrologic modeling of an extreme flood in the guadalupe river in Texas. *J. Am. Water Resour. Assoc*. **2010**, *46*, 881–891.
19. Sharif, H.O.; Sparks, L.; Hassan, A.A.; Zeitler, J.; Xie, H. Application of a distributed hydrologic model to the November 17, 2004 flood of Bull Creek watershed, Austin, Texas. *J. Hydrol. Eng.* **2010**, *15*, 651–657.
20. Sun, X.; Mein, R.G.; Keenan, T.D.; Elliott, J.F. Flood estimation using radar and rain gauge data. *J. Hydrol.* **2000**, *239*, 4–18.
21. Wang, X.; Xie, H.; Sharif, H.; Zeitler, J. Validating NEXRDA MPE and Stage III precipitation products for uniform rainfall on the Upper Guadalupe River Basin of the Texas Hill Country. *J. Hydrol.* **2008**, *348*, 73–86.
22. Smith, J.A.; Seo, D.J.; Baeck, M.L.; Hudlow, M.D. An intercomparison study of NEXRAD precipitation estimates. *Water Resour. Res.* **1996**, *32*, 2035–2045.

23. Young, C.B.; Nelson, B.R.; Bradley, A.A.; Smith, J.A.; Peters-Lidard, C.D.; Kruger, A.; Baeck, M.L. An evaluation of NEXRAD precipitation estimates in complex terrain. *J. Geophys. Res*. **1999**, *104*, 19691–19703.
24. Asadullah, A.; McIntyre, N.; Kigobe, M. Evaluation of five satellite products for estimation of rainfall over Uganda. *Hydrol. Sci. J.* **2008**, *53*, 1137–1150.
25. Bitew, M.M.; Gebremichael, M. Evaluation of satellite rainfall products through hydrologic simulation in a fully distributed hydrologic model. *Water Resour. Res.* **2011**, *47*, W06526.
26. Dai, A.; Lin, X. The frequency, intensity, and diurnal cycle of precipitation in surface and satellite observations over low- and mid-latitudes. *Clim. Dyn.* **2007**, *29*, 727–744.
27. Dinku, T.; Chidzambwa, S.; Ceccato, P.; Connor, S.J.; Ropelewski, C.F. Validation of high-resolution satellite rainfall products over complex terrain. *Int. J. Remote Sens.* **200**8, *29*, 4097–4110.
28. Feidas, H. Validation of satellite rainfall products over Greece. *Theor. Appl. Climatol.* **2010**, *99*, 186–209.
29. Fotopoulos, F.; Makropoulos, C.; Mimikou, M.A. Validation of satellite rainfall products for operational flood forecasting: The case of the Evros catchment. *Theor. Appl. Climatol.* **2011**, *104*, 403–414.
30. Sharif, H.O.; Crow, W.T.; Miller, N.L.; Wood, E.F. Multi-decadal high-resolution hydrological modeling of the Arkansas/Red River basin. *J. Hydrometeorol.* **2007**, *8*, 1111–1127.
31. Hossain, F.; Huffman, G. Investigating error metrics for satellite rainfall data at hydrologically relevant scales. *Am. Meteorol. Soc.* **2007**, *9*, 563–575.
32. Elhassan, A.; Sharif, H.O.; Jackson, T.; Chintalapudi, S. Performance of a conceptual and a physically-based model in simulating the response of a semi-urbanized watershed in San Antonio, Texas. *Hydrol. Process*. **2013**, *27*, 3394–3408.
33. Starks, P.J.; Moriasi, D.N. Spatial resolution effect of precipitation data on swat calibration and performance: Implications for CEAP. *Trans. ASABE* **2009**, *52*, 1171–1180.
34. Collischonn, B.; Collischonn, W.; Tucci, C.E.M. Daily hydrologic modeling in the Amazon basin using TRMM rainfall estimates. *J. Hydrol*. **2008**, *360*, 207–216.
35. Nesbitt, S.W.; Gochis, D.J.; Lang, T.J. The diurnal cycle of clouds and precipitation along the Sierra Madre Occidental observed during NAME-2004: Implications for warm season precipitation estimation in complex terrain. *J. Hydrometeorol.* **2008**, *9*, 728–743.
36. De Goncalves, L.G.G.; Shuttleworth, W.J.; Nijssen, B.; Burke, E.J.; Marengo, J.A.; Chou, S.C.; Houser, P.; Toll, D.L. Evaluation of model-derived and remotely sensed precipitation products for continental South America. *J. Geophys. Res.* **2006**, *111*, doi:10.1029/2005JD006276.
37. Gourley, J.J.; Hong, Y.; Flamig, Z.L.; Wang, J.; Vergara, H.; Anagnostou, E.N. Hydrologic evaluation of rainfall estimates from radar, satellite, gauge, and combinations on Ft. Cobb Basin, Oklahoma. *J. Hydrometeorol*. **2011**, *12*, 973–988.
38. Jiang, S.-H.; Ren, L.-L.; Yong, B.; Yang, X.-L.; Shi, L. Evaluation of high-resolution satellite precipitation products with surface rain gauge observations from Laohahe Basin in northern China. *Water Sci. Eng.* **2010**, *3*, 405–417.
39. Guadalupe-Blanco River Authority: 2008 Basin Summary Report; pp. 32–34. Available online: http://gbra.org/documents/publications/basinsummary/2008d.pdf (accessed on 18 February 2014).

40. Downer, C.W.; Ogden, F.L. GSSHA: Model to simulate diverse stream flow producing processes. *J. Hydrol. Eng.* **2004**, *9*, 161–174.
41. Chintalapudi, S. *Hydrometeorological Analysis of Flooding Events in San Antonio, Texas*; University of Texas at San Antonio: San Antonio, TX, USA, 2008; p. 73.
42. Environmental Modeling Research Laboratory. *Watershed Modeling System [WMS] Version 8.0 Tutorial*; Brigham Young University, Environmental Modeling Research Laboratory: Provo, UT, USA, 2006.
43. Natioanl Oceanic and Atmospheric Administartion. Warm Summer in U.S. Ends with Record Heat in South, Widespread Drought Continues in Southeast, West. Information on Summer-2007 Floods in Texas. Available online: http://www.noaanews.noaa.gov/stories2007/s2917.htm (accessed on 18 February 2014).
44. National Weather Service. A Look Back in History. Available online: http://www.srh.noaa.gov/images/crp/docs/stwj/STWJFall07.pdf (accessed on 18 February 2014).
45. National Aeronautics and Space Administration (NASA). Earth Observatory Image of Tropical Storm Erin. Available online: http://earthobservatory.nasa.gov/NaturalHazards/view.php?id=18911 (accessed on 17 February 2014).
46. Gssha/Main Page. Available online: http://gsshawiki.com/gssha/Main_Page (accessed on 18 February 2014).
47. Seo, D.-J.; Seed, A.; Delrieu, G. *Radar-Based Rainfall Estimation, Chapter in Geophysical Monograph 191, Rainfall: State of the Science*; Testik, F., Gebremichael, M., Eds.; American Geophysical Union: Washington, DC, USA, 2010; pp. 79–104.
48. NASA Mirador Website. Available online: http://mirador.gsfc.nasa.gov/ (accessed on 18 April 2014).
49. Beighley, R.E.; Ray, R.L.; He, Y.; Lee, H.; Schaller, L.; Andreadis, K.M.; Durand, M.; Alsdorf, D.E.; Shum, C.K. Comparing satellite derived precipitation datasets using the Hillslope River Routing [HRR] model in the Congo River Basin. *Hydrol. Process*. **2011**, *25*, 3216–3229.
50. Sorooshian, S.; Kuo-Lin, H.; Xiaogang, G.; Gupta, H.V.; Imam, B.; Braithwaite, D. Evaluation of PERSIANN system satellite-based estimates of tropical rainfall. *Bull. Am. Meteorol. Soc.* **2000**, *81*, 2035–2046.
51. Behrangi, A.; Koulin, H.; Imam, B.; Sorooshian, S. Daytime precipitation estimation using bispectral cloud classification system. *J. Appl. Meteorol. Climatol*. **2010**, *49*, 1015–1031.
52. Vera, T.; Rojas, R.; Zambrano-Bigiarini, M.; Levizzani, V.; de Roo, A. Validation of satellite-based precipitation products over sparsely gauged African river basins. *J. Hydrometeor.* **2012**, *13*, 1760–1783.
53. Zeweldi, D.A.; Gebremichael, M.; Downer, C.W. On cmorph rainfall for streamflow simulation in a small, hortonian watershed. *J. Hydrometeor.* **2011**, *12*, 456–466.